Magnetic Order and Disorder in the Frustrated Quantum Heisenberg Antiferromagnet in Two Dimensions

H.J. Schulz (^{1,*}) T.A.L. Ziman (^{2}) and D. Poilblanc (^{2})

(^{1}) Laboratoire de Physique des Solides (**) , Université Paris-Sud, 91405 Orsay, France
(^{2}) Laboratoire de Physique Quantique (**), Université Paul Sabatier, 31602 Toulouse, France

Abstract. — We have performed a numerical investigation of the ground state properties of the frustrated quantum Heisenberg antiferromagnet on the square lattice ("$J_1 - J_2$ model"), using exact diagonalization of finite clusters with 16, 20, 32, and 36 sites. Using a finite-size scaling analysis we obtain results for a number of physical properties: magnetic order parameters, ground state energy, and magnetic susceptibility (at $q = 0$). In order to assess the reliability of our calculations, we also investigate regions of parameter space with well-established magnetic order, in particular the non-frustrated case $J_2 < 0$. We find that in many cases, in particular for the intermediate region $0.3 < J_2/J_1 < 0.7$, the 16 site cluster shows anomalous finite size effects. Omitting this cluster from the analysis, our principal result is that there is Néel type order for $J_2/J_1 < 0.34$ and collinear magnetic order (wavevector $\mathbf{Q} = (0, \pi)$) for $J_2/J_1 > 0.68$. An error analysis indicates uncertainties of order ± 0.04 in the location of these critical values of J_2. There thus is a region in parameter space without any form of magnetic order. For the unfrustrated case the results for order parameter, ground state energy, and susceptibility agree with series expansions and quantum Monte Carlo calculations to within a percent or better. Including the 16 site cluster, or analyzing the independently calculated magnetic susceptibility we also find a nonmagnetic region, but with modified values for the range of existence of the nonmagnetic region. From the leading finite-size corrections we also obtain results for the spin-wave velocity and the spin stiffness. The spin-wave velocity remains finite at the magnetic-nonmagnetic transition, as expected from the nonlinear sigma model analogy.

1. Introduction

In this paper we consider a simple example of quantum frustrated antiferromagnetism, namely the frustrated spin$-1/2$ Heisenberg model, with Hamiltonian

$$H = J_1 \sum_{\langle i,j \rangle} \mathbf{S}_i \cdot \mathbf{S}_j + J_2 \sum_{\langle i,j' \rangle} \mathbf{S}_i \cdot \mathbf{S}_{j'} \tag{1}$$

The spin operators obey $\mathbf{S}_i \cdot \mathbf{S}_i = 3/4$, and $J_1 = 1$ throughout this paper. The notations $\langle i,j \rangle$ and $\langle i,j' \rangle$ indicate summation over the nearest- and next-nearest neighbor bonds on a square

---

(*) Author for correspondence (e-mail: heinz@solrt.lps.u-psud.fr)
(**) Laboratoires associés au CNRS

lattice, each bond being counted once. While the model has attracted most attention as a simplified model [1] of the effects of doping on copper oxide planes in the high-temperature superconducting copper oxides, it is of rather more general interest. A complete understanding would provide a clear example of answers to several general questions about quantum phase transitions.

The first question is that even in a ground state with rather classical looking symmetry, in this case an antiferromagnet, how do we show unequivocally that the order really is of long range and not simply local? How do we calculate physically measurable correlations without relying on low order perturbation theory? In the present case, for small frustration the appearance, in the limit of infinite size, of spontaneous symmetry breaking is displayed in a relatively simple model. Indeed the renewed interest in the model was because of doubts that the unfrustrated case would display long-range order in the thermodynamic limit. While such doubts are now relatively rare thanks to extensive numerical calculations and tighter rigorous limits for higher spin and lower spin symmetry, [2] there is as yet no rigorous proof for the isotropic spin one-half model in two spatial dimensions. One reason for the present study is to test the quantitative success of ideas of finite size scaling as applied to numerical diagonalizations that are perforce limited to what seem unhelpfully small samples.

The history of finite size effects goes back to Anderson in the nineteen-fifties, [3] who first invoked the fact that the infinite degeneracy of the ground-state with spontaneously broken continuous symmetry must be manifest in a large number of nearly degenerate states in a large but finite system. This idea of a "tower" of states whose degeneracy corresponds to the ultimate symmetry, and whose energy scales determine the long distance parameters of the spontaneously broken model of the infinite system has since been made more precise and less dependent on perturbative concepts in the language of non-linear sigma models [4]. The model we consider here has the advantage over, for example, the triangular or Kagomé antiferromagnets [5,6] in that the classical limit has a simpler unit cell and thus the structure of the towers should be simpler to test. One of our aims here will be to show that it is possible to extract the parameters of the long wavelength physics in the ordered regime. In practice the difficulties of applying finite size studies are still considerable: there are subleading as well as leading corrections which make the ultimate goal of reliable quantitative calculations difficult even here. It is helpful that we may easily stabilize the ordered state to study the disappearance of order in a controlled fashion by applying negative J_2.

A second general question relevant to other quantum phase transitions, is whether the finite size methods developed can be applied all the way to a critical point at which the order may disappear with a continuous transition. The first step is to identify the parameter J_{2c} of this critical point unequivocally; even its existence is still a matter for contention. Indeed some self-consistent spin-wave expansions have been interpreted as indicating a first order transition [7–9], at least for large spin. We shall present results which we feel are rather convincing as to the existence of a critical point and a reasonably accurate estimate of its value.

A third question, separate from the study of ordered antiferromagnetism, is the question of what happens when this order disappears. In the mapping of quantum interacting ground states to thermodynamics of classical models in higher dimension, there is at first sight a difference in that quantum phase transitions tend to show order-order rather than order-disorder transitions. Of course what one means by "order" is crucial to such a distinction. Here an ordered state would be understood to have long range order in a different local order parameter, for example a spin-Peierls dimerization variable or chirality parameter. In this paper we do not discuss in detail the nature of the intermediate state, but we do produce evidence that at least it corresponds to one of zero uniform susceptibility. This is compatible with either the chiral or
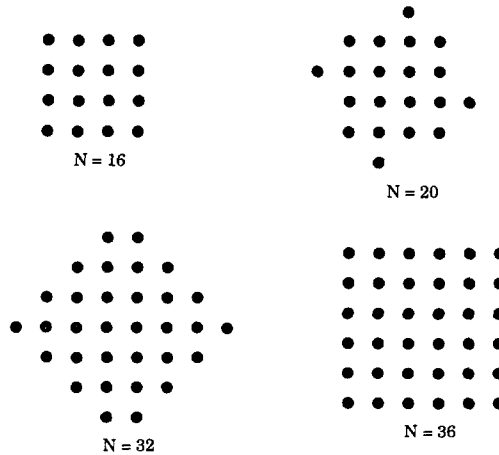
Fig. 1. — The clusters used in this paper.

dimerized phases favored previously [10]. With increasing sample size both phases would have an exponentially vanishing ferromagnetic susceptibility.

We use exact finite-size diagonalization on clusters of $N = 16, 20, 32, 36$ sites (Fig. 1) with periodic boundary conditions. These are all the clusters accessible by our present calculational means that both respect the square symmetry of the lattice and do not frustrate the collinear magnetic state expected at large J_2 (this last condition is violated, for example, for the 18 and 26 site clusters, and more generally whenever N is not an integer multiple of 4). The present study is an improvement of our previous finite-size calculation, [10] which was restricted to the untilted four by four and six by six lattices. We shall see that the inclusion of the intermediate sizes is extremely useful in allowing us to test the consistency of the calculation. The final qualitative conclusions are not drastically changed but estimates of critical parameters in particular are altered. We are also able to articulate questions about whether it is advisable to extrapolate from the sixteen site cluster. In our previous study we had no choice even though the rather special hypercubic property of the 16 site cluster was a concern.

As long as frustration is not too strong, the ground state of the model (1) is expected to have long-range antiferromagnetic order, and then the low-energy long-wavelength excitations are expected to be described by the quantum nonlinear sigma model [11], with action

$$S = \frac{\rho_s}{2} \int d^2r \int_0^\beta d\tau \left[(\nabla \mathbf{n})^2 + \frac{1}{c^2} \left(\frac{\partial \mathbf{n}}{\partial \tau} \right)^2 \right] \tag{2}$$

Here $\mathbf{n} \equiv \mathbf{n}(\mathbf{r}, t)$ is the local orientation of the staggered magnetization, with $|\mathbf{n}| = 1$, c and ρ_s are the spin-wave velocity and spin stiffness, and the inverse temperature β has to be taken to infinity here as we are interested in ground state properties. Lowest order spin-wave theory gives [11,12] $c_0 = \sqrt{2(1 - 2J_2/J_1)}J_1$, $\rho_{s0} = (J_1 - 2J_2)/4$, but there are of course important quantum fluctuation corrections to these quantities. One way to extract these corrections from finite size data will be discussed in Section 3.2 below. We note that the magnetic susceptibility at $\mathbf{q} = 0$ is given by $\chi = \rho_s/c^2$, which in spin-wave theory equals $1/(8J_1)$. A major aim of the paper is to obtain controlled estimates of the different parameters beyond spin-wave theory. A summary of current results for the unfrustrated case can be found in recent review articles [13,14].

2. Numerical Procedures and Results

We wish to find eigenvalues and eigenvectors of the Hamiltonian (1) on large clusters. In order to achieve this, and given that computational power is and will remain limited, it is necessary to use the symmetries of the problem to reduce the size of the corresponding Hilbert space as much as possible. For the $N = 16, 32, 36$ clusters we use:

1. translational symmetry (N operations for an N–site cluster).

2. reflection on horizontal (R_-) and vertical ($R_|$) axes (4 operations). For the $N = 16$ and $N = 36$ cluster, both symmetry axis pass in between rows of spins. However, for $N = 32$, the R_-–axis coincides with the central row of spin (see Fig. 1).

3. if a given eigenstate has the same eigenvalue under R_- and $R_|$, then reflection on the diagonal running from the lower left to the upper right of the cluster ($R_/$) is also a symmetry operation, and can be used to further reduce the size of the Hilbert space by a factor 2. For the 32 site cluster, this operation has to be followed by a translation to remap the cluster onto itself.

4. if the z-component S_z of the total magnetization (which commutes with the Hamiltonian) is zero, then the spin inversion operation $| \uparrow \rangle \leftrightarrow | \downarrow \rangle$ is also a symmetry and leads to a further reduction by a factor 2. In principle a further considerable reduction of the Hilbert space could be achieved by using the conservation of the total spin $\mathbf{S}^2$. However, there does not seem to be any simple way to efficiently incorporate this symmetry.

The point group operations $Id, R_-, R_|, R_/$ generate the point group symmetry C_{4v}. These operations are only compatible with the translational symmetry for states of momentum $\mathbf{Q} = 0$ or $\mathbf{Q} = (\pi, \pi)$. In particular, for our clusters the ground state is always at $\mathbf{Q} = 0$. For the 20 site clusters reflections are not symmetry operations, and we use rather a rotation by $\pi/2$ as generator of the point group. The symmetry group at the interesting momenta $\mathbf{Q} = 0$ or $\mathbf{Q} = (\pi, \pi)$ then is C_4.

We use a basis set characterized by the value of S_{zi} at each lattice site i. An up (down) spin is represented by a bit 1 (0) in a computer word. Thus, a typical spin configuration (e.g. for a linear system of 4 spins) would be represented as

$$| \uparrow \uparrow \downarrow \uparrow \rangle = 1101_2 = 13 \qquad (3)$$

To implement the symmetry, we do not work in this basis, but use rather symmetry-adapted basis states. E.g. to remain in the one-dimensional toy example, instead of (3) we use the normalized basis state

$$\frac{1}{2}(| \uparrow \uparrow \downarrow \uparrow \rangle + | \uparrow \uparrow \uparrow \downarrow \rangle + | \downarrow \uparrow \uparrow \uparrow \rangle + | \uparrow \downarrow \uparrow \uparrow \rangle) = \frac{1}{2}(|13\rangle + |14\rangle + |7\rangle + |11\rangle) \equiv |7\rangle \qquad (4)$$

where the lowest ("*minimal*") integer of the 4 states occurring in (4) is used to represent the state.

Our procedure to determine eigenvectors and eigenvalues proceeds in three steps: i) starting from an arbitrary basis state of given symmetry and S_z, the whole Hilbert space is generated by repeated application of the J_1 part of the Hamiltonian, and the basis set is stored; ii) the Hamiltonian matrix is calculated and stored in two pieces, corresponding to the J_1 and J_2 parts of the Hamiltonian; iii) the matrix is used in a Lanczos algorithm to obtain eigenvalues and eigenvectors of the Hamiltonian. The principal difficulty in steps (i) and (ii) is that application

Table I. — *The number of states in the Hilbert space (n_h) and the number of nonzero off-diagonal matrix elements (n_e) for the clusters used in this paper. The numbers are for states in the A_1 representation (A representation for $N = 20$) at momentum* $\mathbf{Q} = 0$.

N	n_h	n_e
16	107	3664
20	1,321	55,660
32	1,184,480	78,251,988
36	15,804,956	1,170,496,152

of the Hamiltonian to a state represented by a "minimal" integer will of course in general not produce another minimal integer state, but rather a state that needs to be brought into minimal form by the application of a symmetry operation. The trivial solution would be to try out all possible operations. This however would be extremely time consuming (there are 576 symmetry operations for the 36 site cluster!). Instead we use a different procedure [15]: the basis states are coded in a computer word so that the $R_|$ operation corresponds to the exchange of the two halfwords. Each halfword then can be an integer between 0 and $2^{N/2}$ We then create a list specifying for each *halfword* the corresponding minimal state (integer) and the symmetry operation(s) connecting them. The length of this list is relatively moderate (2^{18} at worst), and it can be easily kept in computer memory.

The minimal state corresponding to a given basis state is now determined by looking in this list for the minimal states corresponding to the two halfwords. If necessary, the two halfwords are exchanged (i.e. a $R_|$ operation is performed), so that the smallest of the two halfwords constitutes the high-bit halfword of the resulting state. Finally, the symmetry operation leading to this high-bit halfword is applied to the remaining halfword. In about 80% of the cases this symmetry operation is uniquely determined. In the remaining cases, more than one symmetry operation has to be tried out in order to find the minimal state. However, the extra calculational effort is relatively small: e.g. for $N = 36$, only for about a thousand out of 2^{18} possibilities are there more than eight symmetry operations to be tried out. Using this method for $N = 36$ the CPU time needed to calculate the basis set and the Hamiltonian matrix is approximately 30 min and 90 min., respectively [16]. For the smaller clusters, CPU time requirements are obviously much less. In Table I we show the size of the basis set and the number of non-zero matrix elements for states of A_1 ($N = 16, 32, 36$) or A ($N = 20$) symmetry at $\mathbf{Q} = 0$. These are the subspaces containing the groundstate, apart from the case of relatively large J_2 on the $N = 20, 36$ clusters, where the ground state has point group symmetry B ($N = 20$) or B_1 ($N = 36$). Note that the number of basis states for the larger clusters is very close to the naive expectation $\begin{pmatrix} N \\ N/2 \end{pmatrix} / (16N)$ ($\approx 1.57554 \times 10^7$ for $N = 36$).

The number of matrix elements e.g. for $N = 36$ is still enormous. It is however obvious that the matrix is extremely sparse: on the average, there are fewer than 80 nonzero elements per line, which has in all $15,804,956$ positions. One obviously only wants to store the addresses and values of the nonzero matrix elements. This would still need two computer words per non-zero matrix element, however, this requirement can be further reduced noting that all matrix elements are of the form $H_{i,j} = J_{1,2}(\lambda_i/\lambda_j)I_{i,j}$, where the λ_i are the normalization factors of the symmetrized basis states (like the factor $1/2$ in (4)), and the $I_{i,j}$ are small integers, which in the vast majority of cases equal unity. More specifically, $I_{i,j}$ is the number of times the action of the Hamiltonian on an unsymmetrized basis state $|i\rangle$ creates another unsymmetrized basis

state $|j\rangle$ or a state related to $|j\rangle$ by a symmetry operation. The values of the λ_i intervening in a given matrix element can be easily determined during the calculation, and we thus just store the positions of the unit integer. For the cases where $I_{i,j} = n \neq 1$, the corresponding position is stored n times. Finally, a Cray computer word has 64 bits, and therefore can accommodate two addresses. In this way the whole matrix for the 36 site cluster can be stored in about 5 gigabytes, which is relatively easily available as disk space at the computing facility we are using. Space requirements could be further reduced by a factor 2 using the symmetry of the Hamiltonian matrix, however, this would have lead to a rather important loss of speed in the subsequent matrix diagonalization.

To obtain the groundstate eigenvalue and eigenvector of the Hamiltonian we use the standard Lanczos algorithm, implemented by the Harwell library routine EA15AD. This routine performs rather extensive convergence checks and we thus avoid to perform unnecessary time-consuming Lanczos iterations. The main problem at this level is the use of the still rather large matrix (≈ 5 gigabytes). The matrix clearly does not fit into the main memory of a Cray-2 (2 gigabytes). We therefore store the matrix on disk, and read it in by relatively small pieces, whenever a new piece is needed. This operation can be made computationally efficient by using "asynchronous" input operations, which allow one to perform calculations in parallel with the read-in operation for the next piece of the matrix. Moreover, using more than one input channel simultaneously the read-in operation can be further accelerated. In this way the total time overhang due to the continuous read-in of the matrix can be kept below 20% of total CPU time. To reach a relative accuracy of 10^{-6} for $N = 36$, we need between 40 min. ($J_2 = 0$) and 3 hours ($J_2/J_1 \approx 0.6$, slowest convergence) CPU time. We have performed a number of checks to insure the correctness of the numerical algorithm. The most important one is to calculate the groundstate energy for *ferromagnetic* interaction ($J_{1,2} < 0$), which of course is known to be $(J_1 + J_2)N/2$. However, the numerical calculation in the $S_z = 0$ subspace is nontrivial because the Hilbert space and, up to an overall minus sign, the matrix are of course the same as for the antiferromagnetic case. We also compared our results with previous finite size calculations [17–21] (for $N = 16, 20, 32$) and quantum Monte Carlo results [22] (for $N = 36, J_2 = 0$), and found agreement in all cases. Finally, an independent check of the numerical accuracy of the Lanczos algorithm is provided by starting the Lanczos iterations with different initial vectors. In each case we found a relative accuracy of at least 10^{-6} for the ground state eigenvalues. Similarly, expectation values calculated with the eigenvector are found to have relative accuracy of 10^{-4}. In Table II we list ground state energies of the different clusters for a number of values of J_2. A more complete set of results is displayed in Figure 2.

More important for the following analysis are the values of the **Q**-dependent magnetic susceptibility (or squared order parameter)

$$M_N^2(\mathbf{Q}) = \frac{1}{N(N+2)} \sum_{i,j} \langle \mathbf{S}_i \cdot \mathbf{S}_j \rangle e^{i\mathbf{Q} \cdot (\mathbf{R}_i - \mathbf{R}_j)} \tag{5}$$

Following arguments by Bernu *et al.* [5] we use a normalization by a prefactor $\frac{1}{N(N+2)}$ instead of the usual $1/N^2$. In the thermodynamic limit, these possibilities are obviously equivalent. However, for the relatively small cluster we are using, there are sizeable differences in the results of the finite-size scaling analysis. The choice in equation (5) is essentially motivated by the fact that in a perfect Néel state $M_N^2(\mathbf{Q})$ is entirely size-independent [23]. More generally, this choice eliminates to a certain extent the overly strong contributions from the terms with $i = j$ in equation (5).

Some values of $M_N^2(\mathbf{Q})$ are shown in Table III, and complete curves are in Figure 3. The values displayed (and used in the following analysis) are always expectation values in the *true*

Table II. — *The ground state energy per site for different clusters and different values of J_2 (J_1 is normalized to unity). Where the ground state representation changes with increasing J_2 ($N = 20, 36$), the energies of both relevant representations are given. Boldface indicates the approximate location of changes in the ground state symmetry.*

J_2	16	$20(A)$	$20(B)$	32	$36(A_1)$	$36(B_1)$
−1.00	−1.16457	−1.15103	−0.801770	−1.13251	−1.12922	
−0.50	−0.927249	−0.915408	−0.648275	−0.900134	−0.897626	
0.00	−0.701780	−0.690808	−0.519508	−0.680179	−0.678872	−0.603912
0.10	−0.659817	−0.648444	−0.501316	−0.639048	−0.638096	
0.20	−0.619874	−0.607519	−0.487925	−0.599542	−0.599046	
0.30	−0.582984	−0.568545	−0.479923	−0.562283	−0.562459	
0.40	−0.551147	−0.532381	−0.476480	−0.528379	−0.529745	
0.50	−0.528620	−0.500615	−0.476624	−0.500096	−0.503810	−0.493941
0.55	−0.523594	**−0.487338**	−0.478122	−0.489517	−0.495178	−0.490396
0.60	−0.525896	−0.491633	**−0.491816**	−0.484599	−0.493239	−0.492267
0.65	−0.539382	−0.516444	−0.517029	−0.502147	**−0.506588**	−0.506582
0.70	−0.563858	−0.543309	−0.545677	−0.527741	−0.529951	**−0.530001**
0.80	−0.627335	−0.600092	−0.609595	−0.586871	−0.585428	−0.586487
0.90	−0.696866	−0.659162	−0.677703	−0.651509	−0.645445	−0.649052
1.00	−0.768468	−0.719583	−0.747576	−0.718414	−0.707495	−0.714360
1.20	−0.914286	−0.842827	−0.88967	−0.854910		−0.848364
1.50	−1.13578	−1.03098	−1.10536	−1.06229		−1.05268
2.00	−1.50771	−1.34863	−1.46744	−1.41044		−1.39633

Table III. — *The normalized susceptibility (Eq. (5)) at $\mathbf{Q} = (\pi, \pi)$ and $\mathbf{Q} = (\pi, 0)$ for different clusters and different values of J_2/J_1.*

| J_2/J_1	$M(\pi,\pi)$				$M(\pi,0)$			
	16	20	32	36	16	20	32	36
−1.00	0.26924	0.26002	0.24296	0.23943	0.02778	0.02273	0.01470	0.01316
−0.50	0.26297	0.25221	0.23131	0.22660	0.02780	0.02273	0.01471	0.01316
0.00	0.24580	0.23430	0.20621	0.19879	0.02789	0.02278	0.01476	0.01322
0.10	0.23853	0.22785	0.19745	0.18893	0.02798	0.02284	0.01480	0.01326
0.20	0.22811	0.21949	0.18616	0.17601	0.02818	0.02292	0.01489	0.01335
0.30	0.21212	0.20816	0.17090	0.15800	0.02868	0.02309	0.01506	0.01354
0.40	0.18589	0.19193	0.14887	0.13109	0.03031	0.02348	0.01545	0.01404
0.50	0.14236	0.16693	0.11487	0.09236	0.03709	0.02452	0.01669	0.01594
0.55	0.11276	0.14834	0.09165	0.07062	0.04771	0.02621	0.01880	0.01965
0.60	0.07819	0.02915	0.05113	0.04378	0.07154	0.11508	0.04627	0.03822
0.65	0.04290	0.02015	0.01692	0.01954	0.10897	0.12615	0.10333	0.08167
0.70	0.02092	0.01303	0.01161	0.01232	0.13598	0.13461	0.11321	0.10006
0.80	0.00721	0.00561	0.00520	0.00611	0.15407	0.14383	0.12265	0.11370
0.90	0.00374	0.00302	0.00251	0.00314	0.15930	0.14759	0.12616	0.11925
1.00	0.00236	0.00193	0.00147	0.00183	0.16164	0.14944	0.12759	0.12183
1.20	0.00126	0.00103	0.00072	0.00088	0.16379	0.15118	0.12876	0.12418
1.50	0.00067	0.00055	0.00037	0.00044	0.16507	0.15227	0.12939	0.12553
2.00	0.00033	0.00027	0.00018	0.00021	0.16586	0.15295	0.12977	0.12637
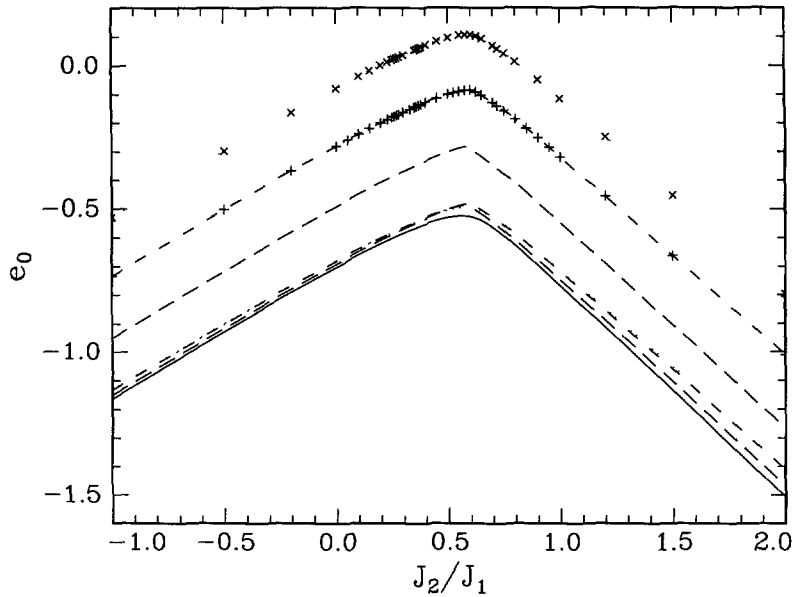
Fig. 2. — The ground state energy per site as a function of J_2/J_1 for $N = 16$ (full line), $N = 20$ (dashed line), $N = 32$ (dash-dotted line), and $N = 36$ (dotted line). For clarity, the curves for $N = 20, 32, 36$ are also displayed shifted upwards by 0.2, 0.4, and 0.6, respectively. For $N = 16, 20$ we have results for J_2/J_1 in steps of 0.01, and only a continuous curve is displayed. For $N = 32, 36$, we have only results at the points indicated, and lines are a guide to the eye.

ground state, e.g. for large J_2 states of symmetry B ($N = 20$) or B_1 ($N = 36$) are used. From the results shown it is quite obvious that the dominant type of magnetic order changes from $\mathbf{Q} = (\pi, \pi)$ at relatively small J_2 (Néel state) to $\mathbf{Q} = (\pi, 0)$ at larger J_2 (collinear state). How exactly this change occurs will be clarified in the following section.

3. Finite-Size Scaling Analysis

3.1. ORDER PARAMETERS. — The results shown in Figure 3 show a transition between a Néel ordered region for $J_2 \lesssim 0.5$ to a state with so-called collinear order (i.e. ordering wavevector $\mathbf{Q} = (\pi, 0)$) at $J_2 \gtrsim 0.6$. To analyze the way this transition occurs in more detail, we use finite-size scaling arguments [24]. In particular, it is by now well established that the low-energy excitations in a Néel ordered state are well described by the nonlinear sigma model. From this one can then derive the finite-size properties of various physical quantities. The quantity of primary interest here is the staggered magnetization $m_0(\mathbf{Q}_0)$ defined by

$$m_0(\mathbf{Q}_0) = 2 \lim_{N \to \infty} M_N(\mathbf{Q}_0) \ , \tag{6}$$

where $\mathbf{Q}_0 = (\pi, \pi)$. The normalization is chosen so that $m_0(\mathbf{Q}_0) = 1$ in a perfect Néel state. The leading finite size corrections to m_0 are given by
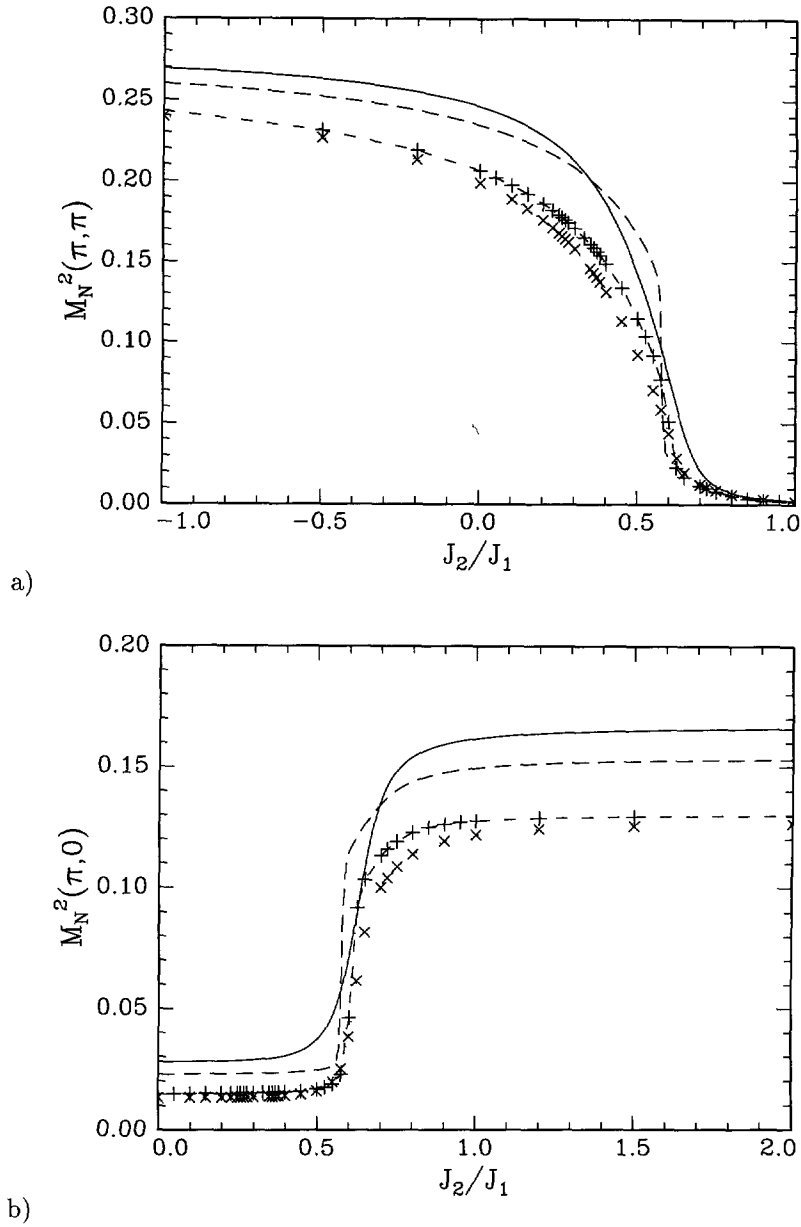
a)

b)

Fig. 3. — The magnetic susceptibility $M(\mathbf{Q})$ at a) $\mathbf{Q} = (\pi, \pi)$ and b) $\mathbf{Q} = (\pi, 0)$. The symbols and linetypes are the same as in Figure 2.

$$
\begin{aligned}
M_N^2(\mathbf{Q}_0) &= \frac{1}{4}m_0(\mathbf{Q}_0)^2 + 1.2416\frac{\kappa_1^2}{\sqrt{N}} + .. \\
&= \frac{1}{4}m_0(\mathbf{Q}_0)^2 \left(1 + \frac{0.6208c}{\rho_s\sqrt{N}} + .. \right) ,
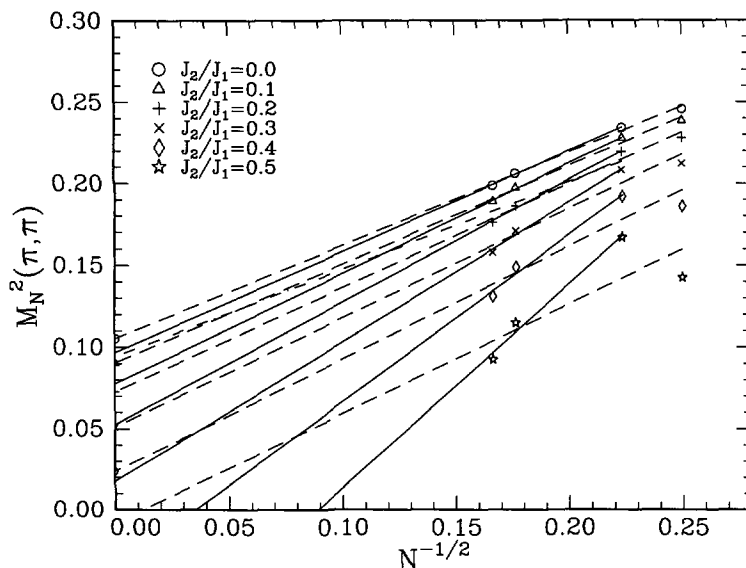\end{aligned}
\tag{7}
$$

Fig. 4. — Finite size results for $M_N^2(\mathbf{Q}_0)$ for different values of J_2. The dashed lines are least squares fits to the data according to equation (7), using all available clusters. The full lines are fits using only $N = 20, 32, 36$. The dash-dotted line is the leading finite size behavior expected at $J_2 = 0$ (see Eq. (7)).

where for the infinite system κ_1 gives the amplitude of the diverging matrix element of the spin operator between the ground state and single magnon states at $\mathbf{Q} \approx \mathbf{Q}_0$.

Least square fits of our finite-size results to equation (7) are shown in Figure 4. For small values of J_2 the scaling law is quite well satisfied: e.g. for $J_2 = 0$ the four data points in Figure 4 very nearly lie on the ideal straight line, and the extrapolated value of the staggered magnetization, $m_0(\mathbf{Q}_0) = 0.649$, is quite close to the best current estimates [22, 25–27], $m_0(\mathbf{Q}_0) = 0.615$ [28]. Using the same type of finite size extrapolations for other values of J_2, we obtain the results indicated by a dashed line in Figure 5.

For $J_2 = 0$, a check on the reliability of our method can be obtained by comparing the numerical results with what one would expect from equation (7), using the rather reliable results for m_0, c, and ρ_s obtained by series expansion techniques [26, 27, 29]. The curve expected from equation (7) is shown as a dash-dotted line in Figure 4. It appears that there are sizeable but not prohibitively large next-to-leading corrections.

Another measure of the reliability of the finite-size extrapolation can be obtained comparing results obtained by the use of different groups of clusters. For negative J_2, i.e. *nonfrustrating interaction*, the values of $m_0(\mathbf{Q}_0)$ are nearly independent of the clusters sizes used, and the results in Figure 5 therefore are expected to be quite accurate. In this region the next nearest neighbor interaction stabilizes the antiferromagnetic order and therefore the staggered magnetization tends to its saturation value unity for large negative J_2. On the other hand, for positive J_2 the interaction is frustrating. In this case, the agreement between different extrapolations is less good. We note however, that in all but two cases the staggered magnetization tends to zero as in a second order phase transition, with a critical value of J_2 between 0.34 and 0.6. The question than arises as to which extrapolation to trust most. In fact, none of the
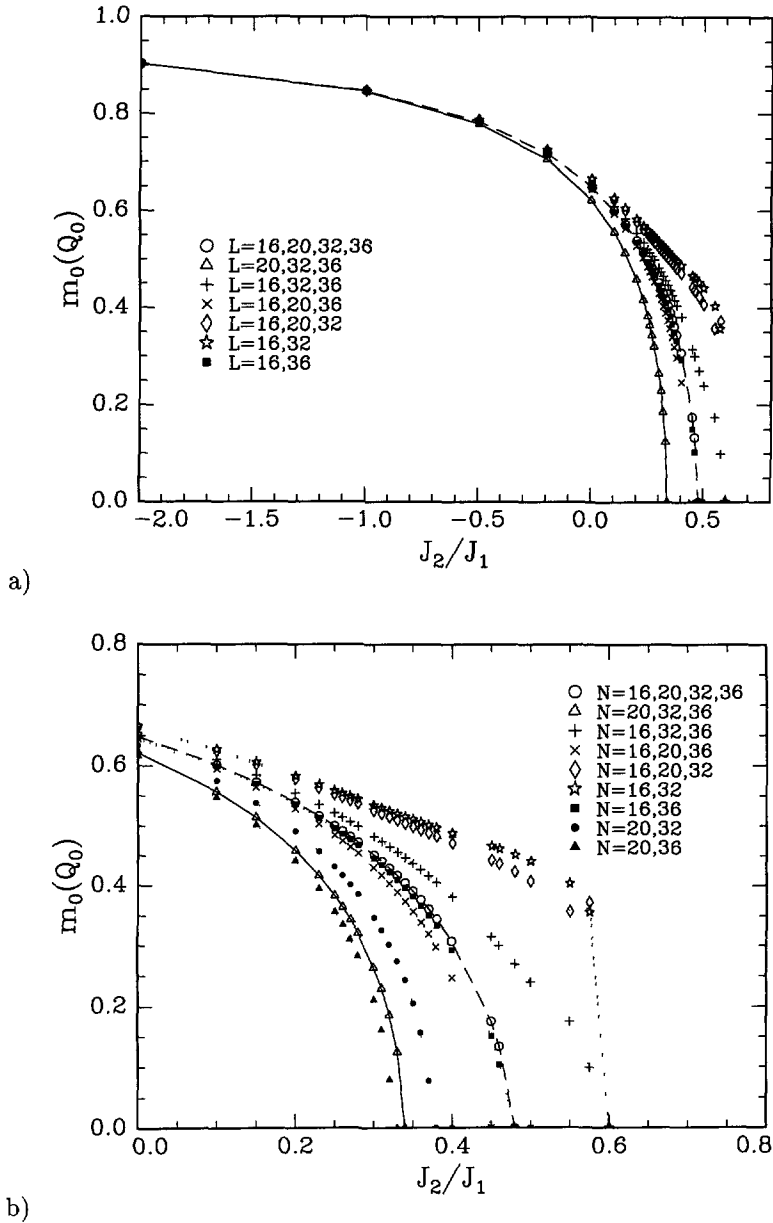
Fig. 5. — The staggered magnetization $m_0(\mathbf{Q}_0)$ as a function of J_2/J_1 using different combinations of clusters (a). In (b) the "critical" region $J_2 > 0$ is shown enlarged.

clusters considered here is free of some peculiarity: for $N = 16$ and $J_2 = 0$, there is an extra symmetry, because with only nearest neighbor interactions this cluster is in fact equivalent to a $2 \times 2 \times 2 \times 2$ cluster on a four-dimensional hypercubic lattice; the $N = 20$ cluster has a lower symmetry than all the others (C_4 instead of C_{4v}); for $N = 20$ and $N = 36$ the ground state changes symmetry with increasing J_2; finally the 20 and 32 site clusters are unusual in

that they are rotated, by different angles, with respect to the lattice directions. *A priori*, one might then argue that the best choice should be the least biased one, including all available clusters. As indicated by the dashed line in Figure 5, this leads to a critical value of J_2 for the disappearance of antiferromagnetic order of $J_{2c} \approx 0.48$.

However, from Figure 4 it is quite clear that for $J_2 \geq 0.35$ the 16 site cluster is highly anomalous in that $M_N^2(\mathbf{Q}_0)$ increases going to the next bigger cluster, whereas in all other cases there is a decrease with increasing size. Clearly, in Figure 4 a much better fit is obtained in this region by omitting the $N = 16$ results, leading to a reduced value, $J_{2c} \approx 0.34$ as indicated by the full line in Figure 5. The anomalous results obtained from the $N = 16, 20, 32$, $N = 16, 32, 36$ and $N = 16, 32$ fits are certainly due to an over-emphasis put onto the $N = 16$ results. Similar anomalous behavior of the 16 site cluster occurs in many cases in the region $0.3 < J_2 < 0.8$, and we therefore consider the results obtained using only $N = 20, 32, 36$ as more reliable. In particular, in this way we find a staggered magnetization of 0.622 at $J_2 = 0$, only about one percent higher than the best current estimate, $m_0(\mathbf{Q}_0) = 0.615$. Beyond the precise value of the critical value J_{2c} at which antiferromagnetic order disappears, the important result here, obtained by the majority of fits, is the existence of a second order transition, located in the interval $0.3 \leq J_2 \leq 0.5$.

One might of course argue that it is not the $N = 16$ but rather the $N = 20$ cluster that is anomalous. However, closer inspection of the data in Figure 4 clearly shows that the $N = 20, 32, 36$ data points remain reasonably well aligned even in the intermediate region $0.3 \leq J_2 \leq 0.8$, whereas the alignment for $N = 16, 32, 36$ is much worse. The $N = 20, 32, 36$ fit also is quite stable: omitting either the $N = 32$ or the $N = 36$ point from it, one obtains only relatively small modifications in the results in Figure 5. On the other hand, starting from $N = 16, 32, 36$ and omitting either of $N = 32$ or $N = 36$ leads to strong modifications. Finally, the $N = 16, 20, 32$ fit (which together with $N = 16, 32, 36$ and $N = 16, 32$ indicates a Néel phase up to $J_2 \approx 0.6$) also is unstable: adding $N = 36$ or replacing $N = 32$ by $N = 36$ leads to drastically modified results.

To obtain a more quantitative criterion for the quality of the different fits, we use standard methods of error estimation, as described for example in reference [30]. The results for $M_N^2(\mathbf{Q}_0)$ in the thermodynamic limit $N \to \infty$ obtained from $N = 16, 20, 32, 36$, $N = 20, 32, 36$, and $N = 16, 32, 36$ are shown in Figure 6 together with the corresponding variances [30] represented as error bars. Extrapolations using other combinations of clusters lead to variances at least twice as big as those for $N = 16, 20, 32, 36$, and therefore are not discussed in the following. The error bars have to be taken with some caution, because errors here certainly are not normally distributed but rather systematic. Nevertheless, the relative size of the error bars certainly is a significant indicator of the quality of the fits. As to be expected from Figure 4, the error bars for the $N = 20, 32, 36$ fit are nearly two times smaller than those obtained from the fit including all points. Similarly, the total χ^2 for $N = 16, 20, 32, 36$ and for $N = 16, 32, 36$ are typically twice as big and 30% bigger than the one obtained from $N = 20, 32, 36$. This rather clearly demonstrates the anomalously large error introduced by the $N = 16$ cluster. Moreover, one observes that for the $N = 16, 20, 32, 36$ and $N = 16, 32, 36$ fits, the Néel order disappears in a region where the error bars are nearly as big as the value of $M_N^2(\mathbf{Q}_0)$ at $J_2 = 0$, indicating a very poor quality of the fit. Only for $N = 20, 32, 36$ does the transition occur in a region of relatively small error bar. Finally, we note that at $J_2 = 0$, we have $M_\infty^2(\mathbf{Q}_0) = 0.105 \pm 0.006, 0.097 \pm 0.004, 0.107 \pm 0.004$ for $N = 16, 20, 32, 36$, $N = 20, 32, 36$, and $N = 16, 32, 36$, respectively, whereas the best current estimate for the staggered magnetization, $m_0(\mathbf{Q}_0) = 0.615$, leads to $M_\infty^2(\mathbf{Q}_0) = 0.095$. Again, only the $N = 20, 32, 36$ extrapolation gives consistent results. In the following, we will therefore mostly rely on the $N = 20, 32, 36$ extrapolations. From Figure 6 we then expect the disappearance of Néel order somewhere in the interval $0.31 < J_2/J_1 < 0.38$, with a best
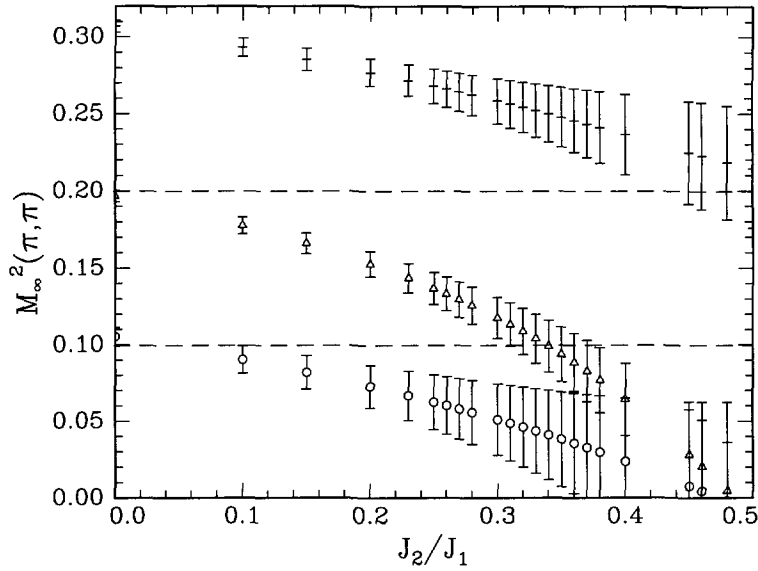
Fig. 6. — Results for the $N \rightarrow \infty$ extrapolation of $M_N^2(\mathbf{Q}_1)$ using $N = 16, 20, 32, 36$ (circles), $N = 20, 32, 36$ (triangles), and $N = 16, 32, 36$ (crosses) with error bars. For clarity the $N = 20, 32, 36$ and $N = 16, 32, 36$ results are shifted upwards by 0.1 and 0.2, respectively.

estimate of 0.34. Similar analyses can also be performed for other quantities calculated below (collinear order parameter, $q = 0$ susceptibility), with similar results. We will therefore not reproduce this type of analysis in detail below.

We now follow the same logic to analyze the behavior for larger J_2, where Figure 3 suggest the existence of magnetic order with ordering wavevector $\mathbf{Q}_1 = (\pi, 0)$. Of course, this state again breaks the continuous spin rotation invariance, and therefore the low energy excitations are described by a (possibly anisotropic) nonlinear sigma model. There is an additional breaking of the discrete lattice rotation symmetry (ordering wavevector $(0, \pi)$ is equally possible), however, this does not change the character of the low-lying excitations. The finite size behavior is entirely determined by the low energy properties, and therefore we expect a finite size formula analogous to equation (7):

$$M_N^2(\mathbf{Q}_1) = \frac{1}{8}m_0(\mathbf{Q}_1)^2 + \frac{\text{const.}}{\sqrt{N}} + .. \tag{8}$$

Here the factor $1/8$ (instead of $1/4$ in (7)) is due to the extra discrete symmetry breaking which implies that finite-size ground states are linear combinations of a larger number of basis states. Moreover, the nonlinear sigma model is anisotropic, because of the spontaneous discrete symmetry breaking of the ordering vector, and consequently a precise determination of the coefficient of the $\sqrt{N}$-term is not straightforward. The important point here is however the N-dependence of the correction term in equation (8).

Least square fits of our numerical results to equation (8) are shown in Figure 7, and the extrapolated collinear magnetization $m_0(\mathbf{Q}_1)$ is shown in Figure 8. For $J_2 \geq 0.8$ equation (8) provides a satisfactory fit to our data, even though not quite as good as in the region $J_2 \leq 0$ in the staggered case, as shown by the spread of different fits in Figure 8 (compare Fig. 5 in the
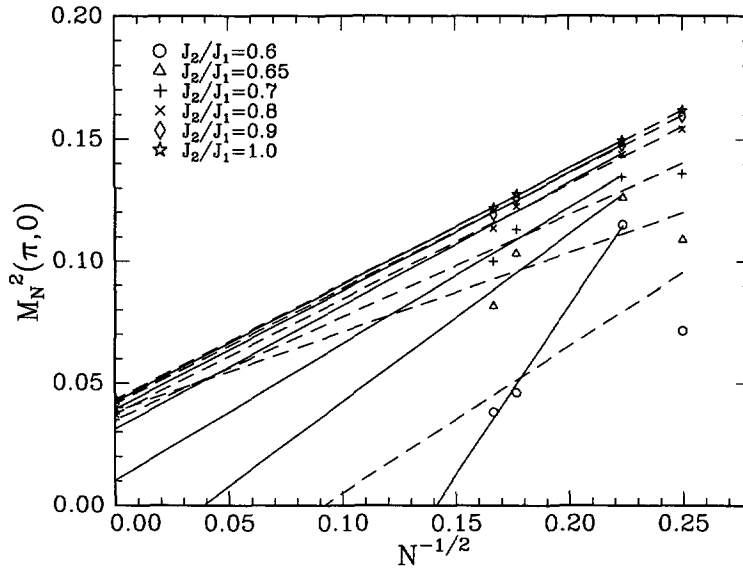
Fig. 7. — Finite size results for $M_N^2(\mathbf{Q}_1)$ for different values of J_2. The dashed lines are least squares fits to the data according to equation (8), using all available clusters. The full lines are fits using only $N = 20, 32, 36$.

region $J_2 \leq 0$). For smaller J_2 there is a wide spread in the extrapolated results, depending on the clusters used. We notice however that for the majority of clusters used, there is a common feature: $m_0(\mathbf{Q}_1)$ remains finite down to $J_2 = 0.65$, and then suddenly drops to zero at $J_2 = 0.6$. This would indicate a *first order transition* to the collinear state somewhere in the interval $0.6 < J_{2c} < 0.65$. This interpretation also seems consistent with the raw data of Figure 3: the increase of $M_N^2(\mathbf{Q}_1)$ around $J_2 = 0.6$ is much steeper than the growth of $M_N^2(\mathbf{Q}_0)$ with decreasing J_2. From the $N = 16, 20, 32, 36$ extrapolation one then obtains a collinear magnetization which is roughly constant above J_{2c} at $m_0(\mathbf{Q}_1) \approx 0.6$. Notice that the first-order character of the transition is *not* due to the level crossings occurring in the $N = 20$ and $N = 36$ clusters: if these clusters are omitted from the extrapolation, the first order character is in fact strongest (cf. Fig. 8).

On the other hand, inclusion or not of the $N = 16$ cluster plays an important role because this cluster shows again anomalous behavior in the region of intermediate J_2: for $J_2 < 0.7$ $M_N^2(\mathbf{Q}_1)$ increases when N increases from 16 to 20, contrary to what equation (8) suggests. Indeed, an error analysis analogous to the one performed for the Néel order parameter again shows a much better quality of the $N = 20, 32, 36$ fit. If one therefore omits the $N = 16$ cluster from the extrapolation, results quite consistent with a second order transition in the interval $0.64 < J_2/J_1 < 0.72$ are obtained, with a best estimate for the critical coupling $J_{2c}/J_1 \approx 0.68$.

It appears that the collinear order parameter tends for large J_2 to a value very close or identical to that of the antiferromagnetic order parameter at $J_2 = 0$. This is in fact not difficult to understand: for $J_2 \gg J_1$ our model represents two very weakly coupled sublattices, with a strong antiferromagnetic coupling J_2 within each sublattice. Consequently, the ground state wave function is to lowest order in J_1/J_2 a product of the wavefunctions of unfrustrated Heisenberg antiferromagnets on the two sublattices. We then obtain $M_N^2(\mathbf{Q}_1, J_2 = \infty) =$
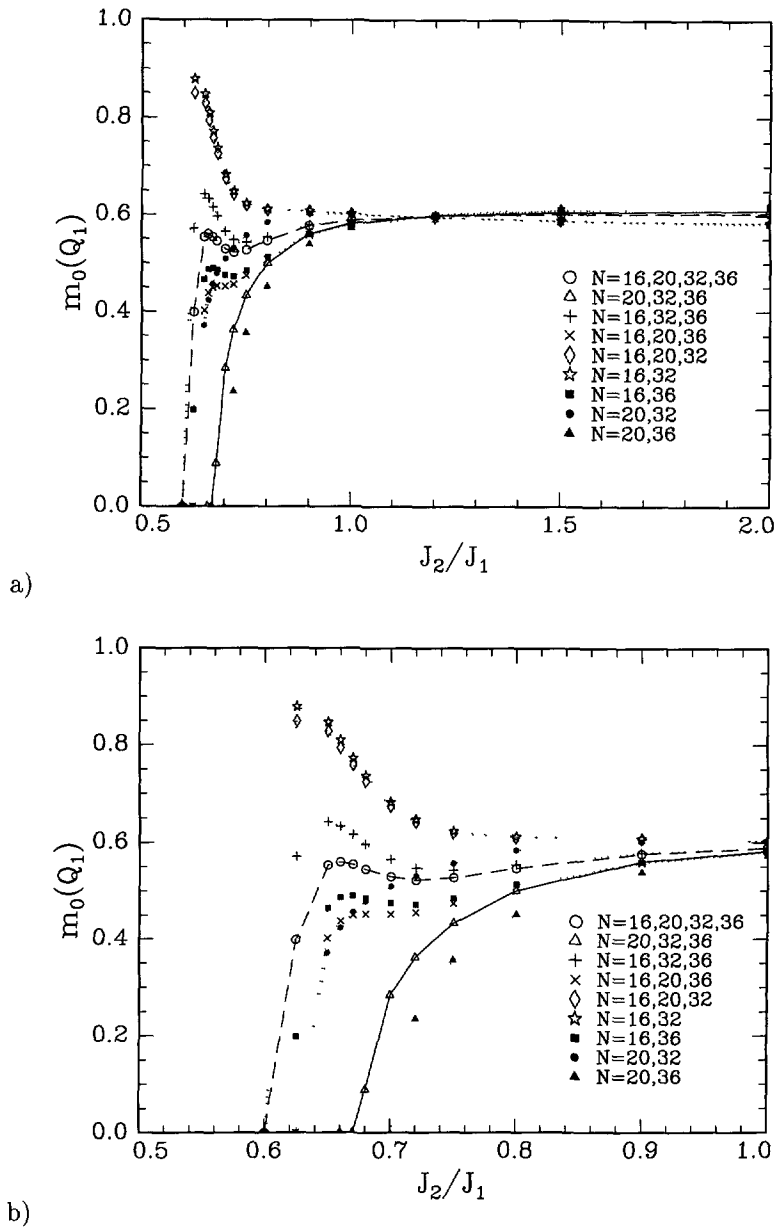
a)

b)

Fig. 8. — The collinear magnetization $m_0(\mathbf{Q}_1)$ as a function of J_2/J_1 using different combinations of clusters (a). In (b) the "critical" region $0.5 \leq J_2 \leq 1.0$ is shown enlarged.

$M_{N/2}^2(\mathbf{Q}_0, J_2 = 0)/2$, and thus from equations (7) and (8) we have the *exact* result

$$\lim_{J_2/J_1 \to \infty} m_0(\mathbf{Q}_1) = m_0(\mathbf{Q}_0)\Big|_{J_2=0} \qquad (9)$$

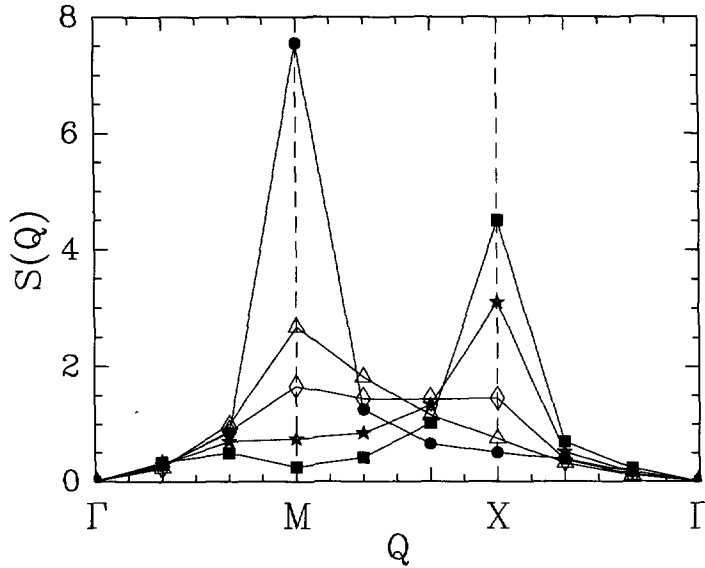Our numerical results do satisfy this relation within the expected (and rather small) uncer-

Fig. 9. — Magnetic structure factor, as obtained from the $N = 36$ cluster, in the Brillouin zone for $J_2/J_1 = 0$ ($\bullet$), 0.55 ($\triangle$), 0.6 ($\diamond$), 0.65 ($\star$), 1 ($\blacksquare$). The points Γ, M, X are $\mathbf{Q} = 0$, $\mathbf{Q}_0$, $\mathbf{Q}_1$, respectively. Note that nowhere there is a maximum at a point different from M or X.

tainties. To obtain this agreement it was however crucial to use the normalization of $M_N^2(\mathbf{Q})$ shown in equation (5). Using a factor $1/N^2$ instead we obtain for large J_2 $m_0(\mathbf{Q}_1) \approx 0.4$, which is far too low. The reason for this is that our extrapolation with $N = 16, 20, 32, 36$ corresponds, for large J_2, to a calculation on two nearly uncoupled and unfrustrated sublattices, each with $N = 8, 10, 16, 18$. On such small lattices, short-range effects are obviously rather large, and therefore the proper normalization of M_N^2 is particularly important.

Beyond quantitative results, the most important conclusion of this analysis is the existence of a finite interval without magnetic long range order: if all available clusters are included in the analysis, this interval is $0.48 \lesssim J_2 \lesssim 0.6$. if, because of the anomalies discussed above one omits the $N = 16$ cluster, the nonmagnetic interval is increased to $0.34 \lesssim J_2 \lesssim 0.68$. The study of the ground state symmetry in this region requires a detailed analysis of a number of different non-magnetic order parameters and will be reported in a subsequent paper. However, at this stage, the magnetic structure factor $S(\mathbf{Q}) = (N+2)M_N^2(\mathbf{Q})$ already gives some valuable information: in fact, as shown in Figure 9, with increasing J_2 the collinear peak at the X point grows and the Néel peak at the M point shrinks, however there never is a maximum at other points. There is thus no evidence for incommensurate magnetic order.

3.2. GROUND STATE ENERGY, SPIN-WAVE VELOCITY, AND STIFFNESS CONSTANT. — The ground state energy per site in the thermodynamic limit can be obtained from the finite-size formula for an antiferromagnet [4,24]

$$E_0(N)/N = e_0 - 1.4372\frac{c}{N^{3/2}} + .. \quad , \tag{10}$$

where c is the spin-wave velocity. Again, in the collinear state, an analogous formula holds, but with c replaced by some anisotropy-averaged value. Fits of our numerical results are
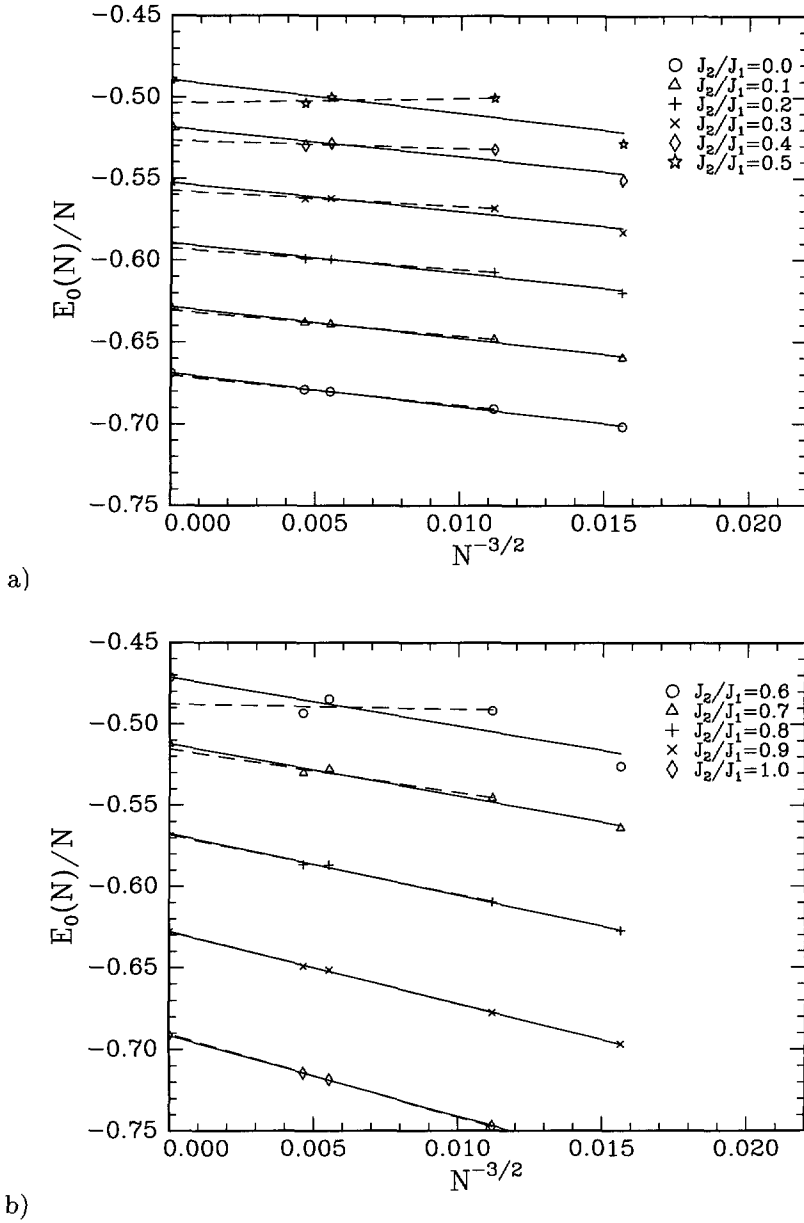
Fig. 10. — Finite size results for the ground state energy per site for different values of J_2. The full lines are least squares fits to the data according to equation (9), using all available clusters. The dashed lines are fits using only $N = 20, 32, 36$.

shown in Figure 10. Away from the "critical" intermediate region, i.e. for $J_2 \leq 0.2$ and $J_2 \geq 0.8$, equation (10) provides a rather satisfying description of the results, in particular if the $N = 16$ cluster is disregarded. The fit is even considerably better than that for the order parameters (compare Fig. 4). This is certainly in large part due to the much weaker finite
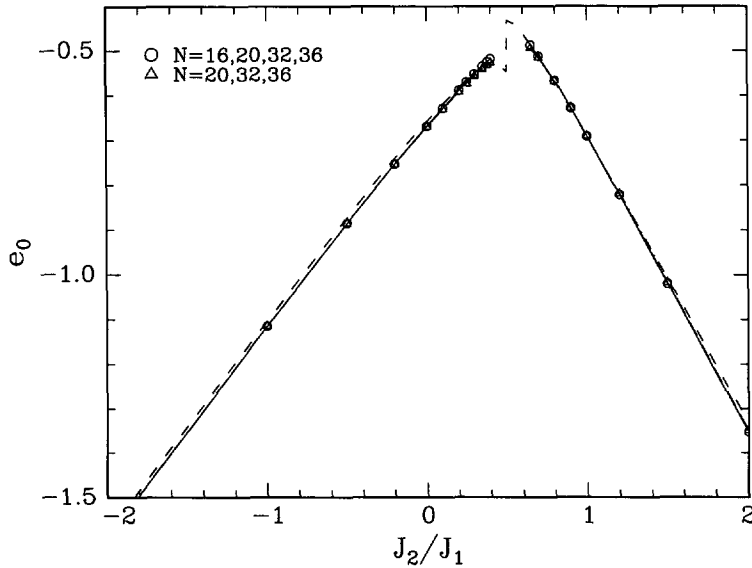
Fig. 11. — Ground state energy per site as obtained from finite size extrapolation using equation (9). In the intermediate region $0.4 < J_2 < 0.65$ the extrapolation can not be used reliably, and no results are shown. Results obtained using different clusters are undistinguishable on the scale of this figure. The dash-dotted line is the spin-wave result, equations (16) and (17).

size correction to the ground state energy, as compared to those for the order parameters. On the other hand, in the intermediate region $0.4 \leq J_2 \leq 0.7$, the fits are not very good. In this region the ground state energy per site is rather irregular, for example there is generally a *decrease* from $N = 32$ to $N = 36$ contrary to what equation (10) suggests. The failure of equation (10) in the intermediate region is of course not surprising, as the analysis of the previous section showed the absence of magnetic order, which implies the non-existence of an effective nonlinear sigma model and therefore the invalidity of the extrapolation formula (10). The result of our extrapolations is shown in Figure 11. Over most of the region shown, results from extrapolations using different clusters are indistinguishable on the scale of the figure. Only close to the critical region is there a spread of about 2 percent in the results. In particular, at $J_2 = 0$ we find values between $e_0 = -0.668$ and $e_0 = -0.670$, very close to the probably best currently available estimate, obtained from large-scale quantum Monte Carlo calculations, of $e_0 = -0.66934$ [25,31].

The amplitude of the leading correction term in equation (10) allows for a determination of the spin-wave velocity c. Results are shown in Figure 12. In this case, there is a wider spread in results. This is certainly not surprising, given that this quantity is derived from the correction term in equation (10). Nevertheless, the agreement between different extrapolations is reasonable for $J_2 \leq 0$. At $J_2 = 0$ and using all clusters we find $c = 1.44J_1$, close to but somewhat lower than the best spin-wave result $c_{SW} = 1.65J_1$. A smaller value is found from the $N = 20, 32, 36$ extrapolation: $c = 1.28$. For positive J_2 the extrapolations give different answers, according to whether the $N = 16$ cluster is included or not. This of course is due to the anomalous behavior of this cluster in the energy extrapolations (see Fig. 10). An important point should however be noticed: independently of the inclusion of the $N = 16$ cluster, at the
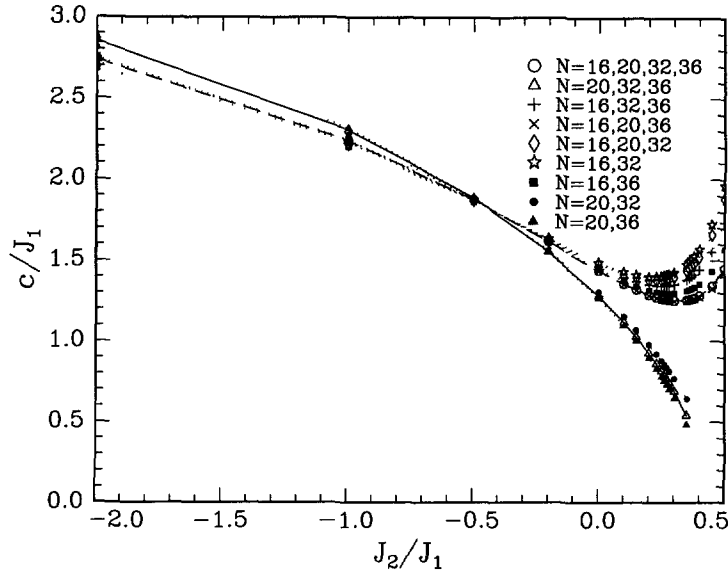
Fig. 12. — The spin wave velocity in the antiferromagnetic state as obtained from finite size extrapolation using equation (9). No results are shown in the region where according to the previous analysis there is no antiferromagnetic order ($J_2 > 0.48$ or $J_2 > 0.34$ according to whether the $N = 16$ cluster is included or not).

critical value J_{2c} for the disappearance of the antiferromagnetic order the spin-wave velocity remains finite.

In principle, better estimates for c might be expected including the known next order correction to equation (10), of order N^{-2} [4]. However, this term predicts a curvature of $E_0(N)/N$ opposite to that obtained in our calculations, and we thus feel use of this higher order term to be inappropriate.

The final parameter in the nonlinear sigma model is the spin stiffness constant ρ_s. It can be found from our finite size results [24]

$$\rho_s = \frac{m_0(\mathbf{Q}_0)^2 c}{8\kappa_1^2} \ , \tag{11}$$

with κ_1 determined from equation (7) [32]. This relation determines the second form of equation (7) above. Results are shown in Figure 13. Again, for the same reasons as before, there is some scatter in the results, because of the use of the correction terms in equations (7) and (10). The results at $J_2 = 0$ ($\rho_s = 0.165$ or 0.125 according to whether $N = 16$ is included or not) is lower than other estimates ($\rho_s \approx 0.18 J_1$) [11,29]. The fact that $\rho_s \to 0$ as $J_2 \to J_{2c}$ is again in agreement with expectations from the nonlinear sigma model analysis, but is of course a trivial consequence of equation (11). A much more reliable way to obtain the spin stiffness is via a direct calculation of the effect of twisted boundary conditions [33].

In the collinear region, there is an additional anisotropy parameter in the effective nonlinear sigma model, and the corresponding effective parameters therefore cannot been obtained straightforwardly from the lowest finite size correction terms.
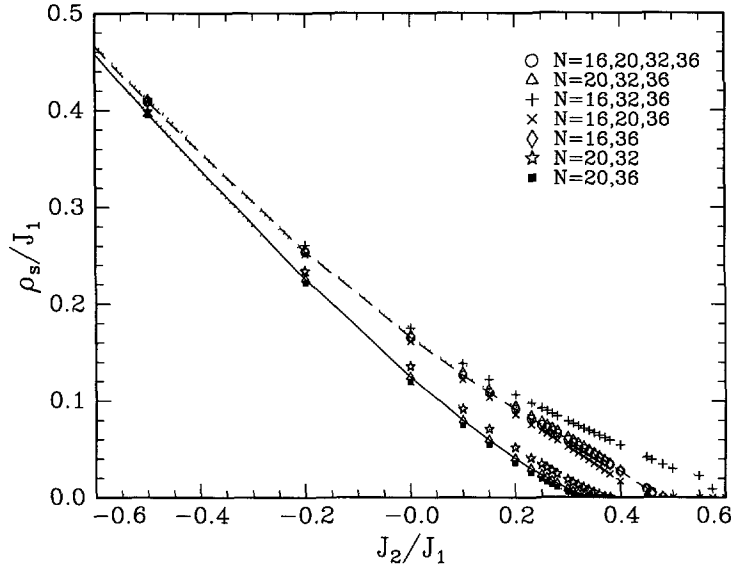
Fig. 13. — The spin stiffness in the antiferromagnetic state as obtained from finite size extrapolation using equation (10). Lines are a guide to the eye.

3.3. SUSCEPTIBILITY AT $q = 0$. — An independent test of the reliability of our results can be obtained by calculating the susceptibility χ: even in an antiferromagnetically ordered state, the $q = 0$ susceptibility is finite, whereas for unconventional states (e.g. dimer or chiral), one has a spin gap and therefore a vanishing susceptibility. The vanishing of the susceptibility can thus be associated with the vanishing of the magnetic order parameter. Moreover, in an antiferromagnetic state one has $\chi = \rho_s/c^2$, and we thus have a consistency check on our calculated values for c and ρ_s. At fixed cluster size one has $\chi(N) = 1/(N\Delta_T)$, where Δ_T is the excitation energy of the lowest triplet state (which has momentum $\mathbf{Q} = (\pi, \pi)$ in an antiferromagnetic state). An extrapolation of $\chi(N)$ to the thermodynamic limit can be performed using the finite-size formula [31, 34] $\chi = \chi(N) - \mathrm{const.}\sqrt{N}$, and results are shown in Figure 14. Again, the $N = 16$ cluster behaves anomalously in that $\chi(N)$ increases going from $N = 16$ to $N = 20$, whereas for bigger clusters there is the expected decrease. In the present case, this anomaly occurs for nearly the whole range $J_2 > 0$. Also, our result for $J_2 = 0$ and using $N = 20, 32, 36$ is $\chi = 0.0671$, very close to both Monte Carlo estimates [31] and series expansion results [26, 27, 29]. We therefore think that the $N = 20, 32, 36$ extrapolation is the most reliable one, and this is confirmed by an error analysis as described above for the Néel order parameter. The vanishing of the susceptibility can be used as an *independent* estimate for the boundary of the Néel region, and this gives a critical value for the disappearance of gapless magnetic excitations and therefore of long-range antiferromagnetic order of $J_{2c} \approx 0.42$, with a lower bound of approximately 0.37. These values are quite close to the estimate we found above by considering the Néel order parameter.

A quantitative comparison of results for the susceptibility obtained either from the excitation gap or from the previously calculated values of c and ρ_s and using $\chi = \rho_s/c^2$ reveals considerable discrepancies (see Fig. 14), even well away from the "critical region" $J_2 \approx 0.4$. The most likely explanation for this is that our calculation of c and ρ_s is based on *corrections* to the leading
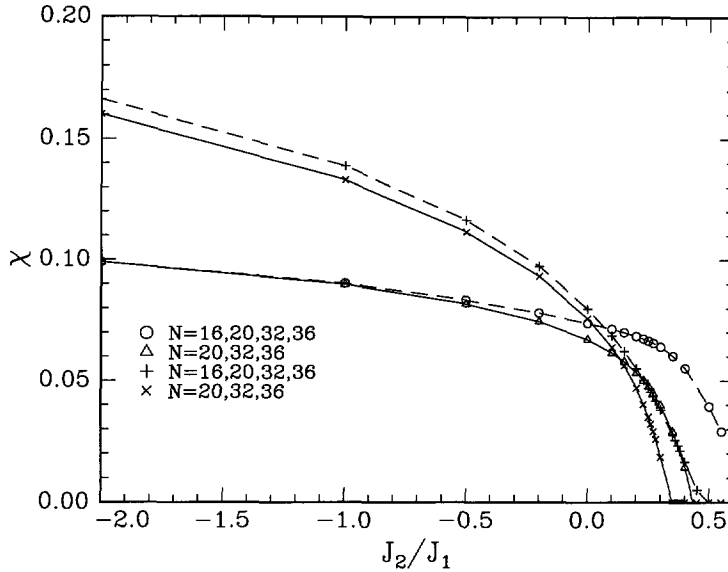
Fig. 14. — The susceptibility in the Néel region as obtained from $\chi = 1/(N\Delta_T)$ (circles and triangles) and from $\chi = \rho_s/c^2$ (crosses) using different extrapolations. As discussed in the text, the $N = 20, 32, 36$ extrapolation is expected to be the most reliable one.

finite-size behavior, whereas χ is obtained directly from the gap. In particular, judging from the case $J_2 = 0$, we probably underestimate the spin wave velocity by quite a bit. The direct estimate of χ is thus expected to be more precise.

An analogous calculation of the susceptibility can be performed in the region of larger J_2, where the lowest excited triplet state is at $\mathbf{Q} = (\pi, 0)$. In this case, because of the double degeneracy of this state, the susceptibility is given by $\chi = 2/(N\Delta_T)$. Because of the lower symmetry of the wavevector, the Hilbert space needed to determine the excited state roughly double in size, and for $N = 36$ has dimension 31561400. We use the same finite-size extrapolation as before, and results obtained for different combinations of cluster sizes are shown in Figure 15. The 16 site cluster again shows rather anomalous behavior and therefore we do not take it into account in these extrapolations. The results then indicate a transition into a nonmagnetic ($\chi = 0$) state at $J_2/J_1 \gtrsim 0.6$, in approximate agreement with what we obtained from estimates of the order parameter above. The decrease of χ with increasing J_2 is not surprising, as for large J_2 the model consists of two nearly decoupled unfrustrated but interpenetrating Heisenberg models, each with exchange constant J_2, and consequently one has $\chi \propto 1/J_2$. What is a bit more surprising is the sharpness of the maximum of χ around $J_2/J_1 = 0.7$.

3.4. COMPARISON WITH SPIN-WAVE THEORY. — Linear spin-wave theory (LSWT) has proven to be a surprisingly accurate description of the ordered state of quantum antiferromagnets even for spin one-half. We here compare our numerical results with that approach. The lowest order spin-wave energies in the antiferromagnetic and collinear state are

$$\omega_{AF}(\mathbf{k}) = 2\{[1 - \alpha(1 - \eta_{\mathbf{k}})]^2 - \gamma_{\mathbf{k}}^2\}^{1/2} , \qquad (12)$$

$$\omega_{coll}(\mathbf{k}) = \{(2\alpha + \gamma_x)^2 - (2\alpha\eta_{\mathbf{k}} + \gamma_y)^2\}^{1/2} , \qquad (13)$$
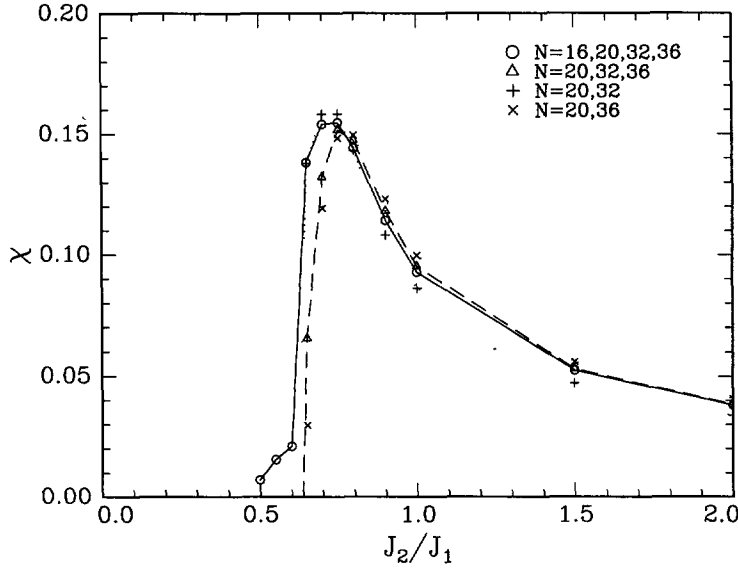
Fig. 15. — The susceptibility in the collinear region as obtained from $\chi = 2/(N\Delta_{\mathrm{T}})$ using different extrapolations. As discussed in the text, the $N = 20, 32, 36$ extrapolation is expected to be the most reliable one.

where $\alpha = J_2/J_1$, $\gamma_\alpha = \cos k_\alpha$, $\gamma_{\mathbf{k}} = (\gamma_x + \gamma_y)/2$, and $\eta_{\mathbf{k}} = \gamma_x \gamma_y$. In LSWT, the order antiferromagnetic and collinear order parameters then are given by [11,35]

$$m_0(\mathbf{Q}_0) \;=\; 1 - \frac{1}{4\pi^2} \int \mathrm{d}^2 k \frac{1 - \alpha(1 - \eta_{\mathbf{k}})}{\omega_{\mathrm{AF}}(\mathbf{k})} \tag{14}$$

$$m_0(\mathbf{Q}_1) \;=\; 1 - \frac{1}{8\pi^2} \int \mathrm{d}^2 k \frac{2\alpha + \gamma_x}{\omega_{\mathrm{coll}}(\mathbf{k})} \tag{15}$$

where the integration is over the full first Brillouin zone. A comparison of our results with this approach is shown in Figure 16. For the antiferromagnetic order parameter, we observe very satisfying agreement. What is slightly disturbing here is that inclusion of the next order $(1/S^2)$ correction to equation (14) [11] actually makes the agreement worse, even for negative J_2 where the next-nearest neighbor interaction stabilizes the order and spin-wave theory therefore should be increasingly reliable. For example, for $J_2 = -J_1$ these corrections lead to [36] $m_0(\mathbf{Q}_0) = 0.775$, whereas we find $m_0(\mathbf{Q}_0) = 0.846$. To which extent higher-order spin wave theory can be used systematically even in this region thus seems unclear. For the more interesting case of positive J_2, higher corrections to spin-wave theory give more and more strongly diverging results as $J_2 \to 0.5$, and it is not clear how any useful information can be obtained from these higher order corrections in the frustrated case. We therefore limit our comparison here to linear spin-wave theory.

For the collinear state at large J_2, there is a similar good agreement between spin-wave theory and our results, except for the immediate vicinity of the transition to the nonmagnetic state. We note that the spin-wave results (14) and (15) do satisfy the exact result (9).
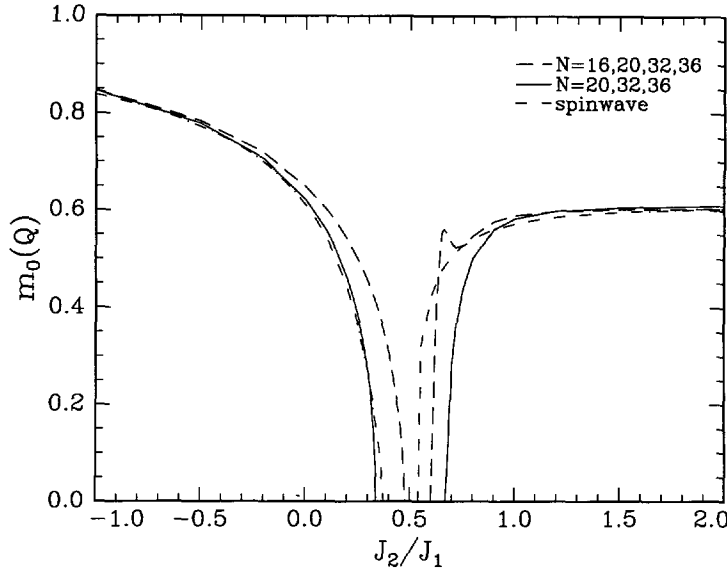
Fig. 16. — Comparison of our finite size fits for the antiferromagnetic and collinear order parameters (left and right curves, respectively) with linear spin wave theory.

The ground state energy per site is given in lowest order spin-wave theory by [36,37]

$$e_0 = \frac{3}{2}(\alpha - 1) + \frac{1}{8\pi^2} \int d^2k \, \omega_{AF}(k) \, , \tag{16}$$

$$e_0 = -\frac{3}{2}\alpha + \frac{1}{8\pi^2} \int d^2k \, \omega_{coll}(k) \tag{17}$$

for the antiferromagnetic and collinear state, respectively. As can be seen in Figure 11, these results are rather close to our finite-size extrapolations. Nevertheless, there is a significant discrepancy: e.g. for $J_2 = 0$ the spin-wave result is $e_0 = -0.6579$, compared to the presumably best estimate from large scale Monte Carlo calculations [25,31], $e_0 = -0.66934$. On the other hand, as discussed above, our finite size extrapolation gives values very close to this. It would thus seem that, as far as the ground state energy is concerned, finite-size extrapolation is more precise than linear spin-wave theory.

Comparing our results for the spin-wave velocity and spin stiffness (Fig. 12 and 13) to the LSWT results $c = \sqrt{2(1 - 2J_2/J_1)}J_1$ and $\rho_s = (J_1 - 2J_2)/4$, one finds rather sizeable discrepancies, both for ρ_s and for c. Nevertheless, the functional form for large negative J_2 seems to be correct. However, here a detailed comparison seems not particularly useful as LSWT results themselves are rather imprecise (as shown e.g. by the large renormalization of the susceptibility at $J_2 = 0$).

4. Summary and Discussion

In this paper we have reported detailed finite-size calculations on the frustrated spin$-1/2$ antiferromagnetic Heisenberg model on the square lattice. Using finite-size extrapolation formulae,

Table IV. — *Comparison of our results at $J_2 = 0$ obtained from the $N = 16, 20, 32, 36$ and $N = 20, 32, 36$ extrapolations with previous estimates from series expansions and quantum Monte Carlo calculations. A more complete compilation of previous results can be found in review articles [13, 14].*

	e_0	$m_0(\mathbf{Q}_0)$	χ
$N = 16, 20, 32, 36$	−0.6688	0.649	0.0740
$N = 20, 32, 36$	−0.6702	0.622	0.0671
series expansions (See Refs. [26] and [27])	−0.6696	0.614	0.0659
quantum Monte Carlo (See Refs. [22], [31], and [25])	−0.6693	0.615	0.0669

we derived results for a number of physical properties. The most important finding seems to be the existence of a region of intermediate second nearest neighbor coupling J_2 where no magnetic order, antiferromagnetic, collinear or otherwise, exists. The location of the boundaries of this nonmagnetic region depends on the cluster size involved in the estimate. For $N = 16, 20, 32, 36$ we find the interval $0.48 \leq J_2/J_1 \leq 0.6$ to be nonmagnetic, whereas with $N = 20, 32, 36$ this interval is larger: $0.34 \leq J_2/J_1 \leq 0.68$. Given the irregular behavior of the $N = 16$ cluster we often found above, in particular in the region of intermediate J_2, the second estimate would appear to be the more reliable one. In any case, independently of which extrapolation one prefers, there is a nonmagnetic interval.

Beyond the existence of a nonmagnetic region, we have also obtained quantitative estimates for a number of fundamental physical parameters in the magnetically ordered states, antiferromagnetic for small or negative J_2, collinear for large positive J_2. The accuracy of these estimates can best be assessed by comparing with the unfrustrated case $J_2 = 0$, for which case there are currently rather precise results available, mainly from large-scale Monte Carlo calculations and series expansions. A summary of our results, together with other recent data, is given in Table IV. Our results for the ground state energy, the antiferromagnetic order parameter, and the susceptibility agree to within a percent or better, with the best currently available numbers. Finally, our estimates for the spin-wave velocity and the spin stiffness are rather imprecise. This is certainly mainly due to the fact that these quantities are obtained from the amplitudes of the leading correction to the asymptotic large-size behavior of the ground state energy and the order parameter susceptibility, and these corrections are almost certainly estimated less precisely than the leading terms. A much improved and rather precise estimate of the spin stiffness can be obtained directly calculating the effect of twisted boundary conditions on the ground state energy [33].

We found it instructive to also investigate regions where magnetic order is well-established, i.e. $J_2 \leq 0$ for the antiferromagnetic case and $J_2 \geq J_1$ for the collinear case. In these regions we find that the finite-size formulae like (7) and (10) provide an excellent fit to our numerical results. The progressive worsening of the quality of the fits as the intermediate region is approached certainly is consistent with the existence of a qualitatively different ground state in that region. If on the contrary the transition between antiferromagnetic and collinear order occurred *via* a strong first order transition (as suggested by some approximate theories, see below), no such progressive worsening is expected. We also notice in this context that the $N = 16$ cluster is systematically the one exhibiting the largest deviations from the expected behavior, probably due to its unusually high symmetry. We thus feel that estimates ignoring this cluster may be more reliable.

Another way to assess the consistency of the finite-size extrapolations we are using is to
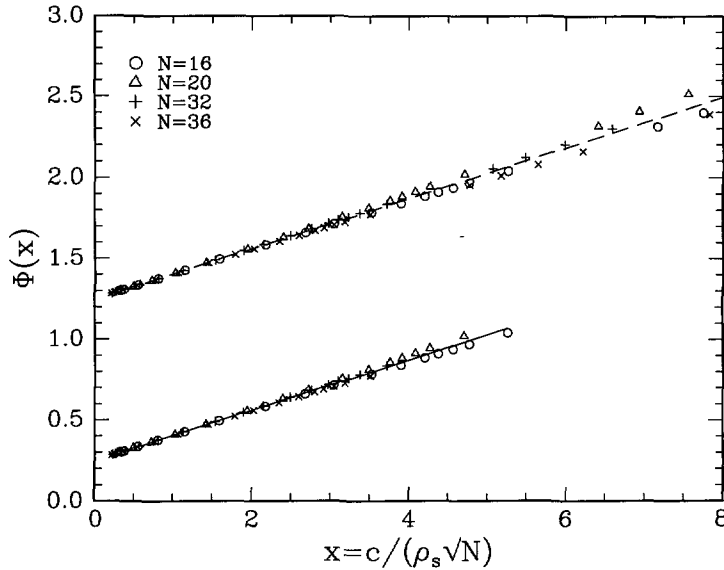
Fig. 17. — Scaling plot of $\Phi(x) = M_N^2(\mathbf{Q}_0)/m_0(\mathbf{Q}_0)^2$ as a function of the variable $x = c/(\rho_s\sqrt{N})$, using the $N = 20, 32, 36$ (lower curve) and $N = 16, 20, 32, 36$ (upper curve) extrapolations for c and ρ_s. For clarity, data for the $N = 16, 20, 32, 36$ extrapolation are shifted upward by 1 unit. The straight lines represent the spin wave result $\Phi(x) = (1 + 0.6208x)/4$

verify the underlying scaling hypothesis *via* a "scaling plot". The fundamental constants c and ρ_s of the nonlinear sigma model define a length scale c/ρ_s, and if finite size scaling is verified one therefore expects all finite size corrections to be universal functions of the variable $x = c/(\rho_s\sqrt{N})$. In particular, for the order parameter susceptibility we expect

$$M_N^2(\mathbf{Q}_0) = m_0(\mathbf{Q}_0)^2 \Phi(x) \tag{18}$$

Combining the second form of equation (7), equation (11), and this definition, the small-x expansion of the scaling function is $\Phi(x) = (1+0.6208x)/4$. Plots of our results for $M_N^2(\mathbf{Q}_0)$ as a function of the scaling variable x are shown in Figure 17. One sees that for the $N = 20, 32, 36$ extrapolation the plot is nearly perfect in that nearly all data points are collapsed onto a single curve. The only points that show a significant deviation are those obtained for $N = 16$ close to the phase transition to the nonmagnetic state. This of course is nothing but a manifestation of the anomalous behavior of this cluster already found previously. The behavior for the $N = 16, 20, 32, 36$ extrapolation is clearly less satisfying. A similar scaling plot for the ground state energy produces even better results, due to the better convergence of the corresponding finite-size formula (10).

A scaling plot like Figure 17 permits to assess the consistency of data obtained for clusters of different sizes, however, the form of the scaling function itself is obviously less significant as the coefficients c and ρ_s entering the definition of the scaling variable x are calculated assuming finite-size formulae like (7) and (10) to be valid, i.e. implicitly *assuming* the form $\Phi(x) = (1 + 0.6208x)/4$. An *independent* estimate of Φ can in principle be obtained using independent estimates for c and ρ_s. We do not have currently such an estimate for ρ_s, however we can use our independent results for the susceptibility (Fig. 14) to rewrite the scaling variable
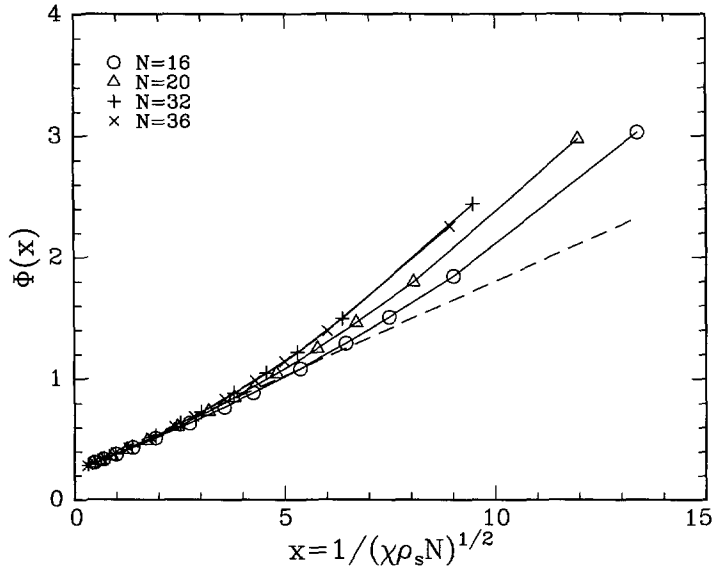
Fig. 18. — Scaling plot of $\Phi(x) = M_N^2(\mathbf{Q}_0)/m_0(\mathbf{Q}_0)^2$ as a function of the variable $x = 1/(\chi\rho_s N)^{1/2}$, using the $N = 20, 32, 36$ results for χ (see Fig. 14) and the $N = 20, 32, 36$ extrapolation for ρ_s. The dashed line represents the spin wave result $\Phi(x) = (1 + 0.6208x)/4$

as $x = 1/\sqrt{\chi\rho_s N}$. The plot obtained using estimates for ρ_s and χ from $N = 20, 32, 36$ is shown in Figure 18. The collapse of data obtained for different sizes and values of J_2 is not as satisfactory as in the previous case, however, this is certainly related to the fact that here we use a second independently estimated quantity, namely χ. Still, for $x \lesssim 5$, the collapse is rather good, showing the consistency of our analysis in this region. For the larger clusters, this region corresponds to $J_2/J_1 \leq 0.25$, i.e. it extends rather close to the transition which occurs at $J_2/J_1 \approx 0.34$. For small x the calculated scaling function essentially agrees with the spin–wave results shown by the dashed line in Figure 18. For $x \gtrsim 5$, there are discrepancies between results obtained from $M_N^2(\mathbf{Q}_0)$ for different N. This probably indicates that at least for the smaller clusters, finite size effects become so important that it is no more sufficient to include the lowest order finite size corrections only. The fact that the numerically found scaling function is larger than the spin–wave approximation is not entirely unexpected: in fact, for large x, i.e. in the critical region, one would expect $\Phi(x) \propto x^{1+\eta}$, where η is the correlation exponent of the three-dimensional Heisenberg model. However, we doubt that what we observe in Figure 18 is actually a critical effect. First, the numerical value [38] of $\eta = 2 - (\gamma/\nu)$ is very small: $\eta \approx 0.03$, and one thus expects an extremely smooth crossover. Moreover, in Figure 18 we have used the independently calculated susceptibility (see Fig. 14) which goes to zero only at $J_2/J_1 \approx 0.42$, rather than at $J_2/J_1 \approx 0.34$ where our estimated staggered magnetization vanishes. Consequently, the abscissae of the data points in Figure 18 are underestimated, i.e. the data in Figure 18 overestimate the true $\Phi(x)$.

The $J_1 - J_2$ model we have studied here has been investigated previously by number of techniques. Previous finite-size studies [17,18] found some indication of an intermediate phase without magnetic order, however due to the limitation to $N = 16$ and 20 only, it was impossible to make extrapolations to the thermodynamic limit and to arrive at quantitative statements.

Our own previous study [10], using $N = 16$ and 36, produced results very similar to our current best estimates. However, due to the larger number of clusters we now use (and due to the possibility to ignore the anomalous $N = 16$ cluster), we feel that our conclusions are considerably more reliable.

Lowest order spin-wave theory [35] produces a phase diagram very similar to ours (see Fig. 16). On the other hand, higher order (in $1/S$) calculations do not seem to be very useful, due to increasingly strong singularities at $J_2 = J_1/2$. It has been attempted to include higher order corrections using a selfconsistently modified spin-wave theory [7,8]. These calculations as well as the closely related Schwinger boson approach [9] produce a first order transition between Néel and collinear state. Our results here seem to exclude this possibility: a first order transition (unless it is very weakly first order) would mean that for example the finite-size scaling law for the squared order parameter should be well satisfied all the way to the transition. This is clearly not what is observed in the regions of intermediate J_2 in Figures 4 and 7. A combination of Schwinger boson results and a renormalization group calculation [12] gives on the other hand a second order transition from the Néel state to a magnetically disordered state, at $J_{2c}/J_1 = 0.15$ [39]. However, the applicability of these approaches to an $S = 1/2$ system is hard to judge, mainly due to the absence of a small parameter that would make a systematic expansion possible.

Quantum Monte Carlo methods are plagued with the sign problem for frustrated spin systems. Nevertheless, conclusions very similar to the modified spin wave calculations have been reached recently using a quantum Monte Carlo method [40]. However, these results have rather large error bars and in some cases, in particular in the region of intermediate J_2, are in disagreement with our present exact results. The validity of these results thus appears doubtful to us.

Another approach has been via series expansion methods around a lattice covered by isolated dimers [41]. Expanding around a columnar arrangement of dimers, these authors find a phase diagram very similar to ours, at least as far as magnetic order is concerned. However, these results are not without ambiguity: expanding around a staggered dimer arrangement, there appears to be a first order transition between Néel and collinear states. The results of this method thus appear to be biased by the starting point of the expansion.

The most obvious question left open by the present study is the nature of the ground state in the intermediate nonmagnetic region. Work extending our previous analysis [10] is in progress and will be reported in a subsequent publication. It would also be interesting to investigate dynamical correlations functions, in particular in the vicinity of the critical point of the Néel state, $J_{2c} = 0.34$. One thus might gain additional insight into dynamical properties at a quantum critical point [42,43]. Finally, one might also try to extend the size of the available clusters, in order to achieve better accuracy and reliability. The next useful cluster has 40 sites, and should be tractable in the near future. However, the next step then would be a cluster of 52 sites which would require computational means both in memory size and speed three or four orders of magnitude more powerful than what is currently available. A viable alternative to increase the size of the tractable clusters might be to combine the exact solution of moderately big clusters with Monte Carlo type approaches.

Acknowledgments

References

[1] Inui M., Doniach S. and Gabay M., *Phys. Rev. B* **38** (1988) 6631.

[2] Kubo K. and Kishi T., *Phys. Rev. Lett.* **61** (1987) 2585.

[3] Anderson P.W., *Phys. Rev.* **86** (1952) 694.

[4] Hasenfratz P. and Niedermayer F., *Z. Phys. B* **92** (1993) 91.

[5] Bernu B., Lhuillier C. and Pierre L., *Phys. Rev. Lett.* **69** (1992) 2590.

[6] Azaria P., Delamotte B. and Mouhanna D., *Phys. Rev. Lett.* **68** (1992) 1762.

[7] Takahashi M., *Phys. Rev. B* **40** (1989) 2494.

[8] Nishimori H. and Saika Y., *J. Phys. Soc. Jpn.* **59** (1990) 4454.

[9] Mila F., Poilblanc D. and Bruder C., *Phys. Rev. B* **43** (1991) 7891.

[10] Schulz H.J. and Ziman T.A.L., *Europhys. Lett.* **18** (1992) 355.

[11] Chakravarty S., Halperin B.I. and Nelson D.R., *Phys. Rev. B* **39** (1989) 2344.

[12] Einarsson T. and Johannesson H., *Phys. Rev. B* **43** (1991) 5867.

[13] Manousakis E., *Rev. Mod. Phys.* **63** (1991) 1.

[14] Barnes T., *Int. J. Mod. Phys. C* **2** (1991) 659.

[15] We are extremely grateful to L. Pierre for suggesting this method.

[16] On a recently available Cray C98, CPU times cited here typically are decreased by a factor six.

[17] Dagotto E. and Moreo A., *Phys. Rev. Lett.* **63** (1989) 2148.

[18] Figueiredo F. *et al.*, *Phys. Rev. B* **41** (1990) 4619.

[19] Lin H.Q., *Phys. Rev. B* **42** (1990) 6561.

[20] Poilblanc D., Gagliano E., Bacci S. and Dagotto E., *Phys. Rev. B* **43** (1991) 10970.

[21] Poilblanc D. and Dagotto E., *Phys. Rev. B* **45** (1991) 10111.

[22] Runge K.J., *Phys. Rev. B* **45** (1992) 7229.

[23] We are grateful to C. Lhuillier for pointing this out to us.

[24] Neuberger H. and Ziman T.A.L., *Phys. Rev. B* **39** (1989) 2608.

[25] Wiese U.-J. and Ying H.-P., *Z. Phys. B* **93** (1994) 147.

[26] Singh R.R.P., *Phys. Rev. B* **39** (1989) 9760.

[27] Weihong Z., Oitmaa J. and Hamer C.J., *Phys. Rev. B* **43** (1991) 8321.

[28] Using a prefactor $1/N^2$ instead of $1/(N(N+2))$ in equation (5), we find $m_0(\mathbf{Q}_0) = 0.554$ and $m_0(\mathbf{Q}_0) = 0.532$ using $N = 16, 20, 32, 36$ and $N = 20, 32, 36$, respectively (see also Ref. [10]). The correct prefactor thus considerably improves the precision of the estimates. Using the $1/N^2$ prefactor also shifts the critical value for the disappearance of Néel order down by approximately 0.05.

[29] Singh R.R.P. and Huse D., *Phys. Rev. B* **40** (1989) 7247.

[30] Press W.H., Flannery B.P., Teukolsky S.A. and Vetterling W.T., Numerical Recipes in C (Cambridge University Press, Cambridge, 1988) p. 523 ff.

[31] Runge K.J., *Phys. Rev. B* **45** (1992) 12292.

[32] Note that this is the correct form, as was used in reference [10]. In reference [24] the relation was misquoted.

[33] Einarsson T. and Schulz H.J., *Phys. Rev. B* **51** (1995) 6151.

[34] Fisher D.S., *Phys. Rev. B* **39** (1989) 11783.

[35] Chandra P. and Doucot B., *Phys. Rev. B* **38** (1988) 9335.

[36] Einarsson T., private communication.

[37] Bergomi L., Thesis (Orsay), unpublished.

[38] Peczak P., Ferrenberg A.M. and Landau D.P., *Phys. Rev. B* **43** (1991) 6087.

[39] Einarsson T., Fröjdh P. and Johannesson H., *Phys. Rev. B* **45** (1992) 13121.

[40] Nakamura T. and Hatano N., *J. Phys. Soc. Jpn.* **62** (1993) 3062.

[41] Gelfand M.P., Singh R.R.P. and Huse D.A., *Phys. Rev. B* **40** (1989) 10801.

[42] Sachdev S. and Ye J., *Phys. Rev. Lett.* **69** (1992) 2411.

[43] Chubukov A.V., Sachdev S. and Ye J., preprint.